Experimental determination of the symmetry energy of a low density nuclear gas

S. Kowalski,[*] J. B. Natowitz, S. Shlomo, R. Wada, K. Hagel, J. Wang,[†] T. Materna, Z. Chen, Y. G. Ma,[‡]
L. Qin, and A. S. Botvina[§]
Cyclotron Institute, Texas A&M University, College Station, Texas 77843, USA

D. Fabris, M. Lunardon, S. Moretto, G. Nebbia, S. Pesente, V. Rizzi, and G. Viesti
INFN and Dipartimento di Fisica dell' Universitá di Padova, I-35131 Padova, Italy

M. Cinausero and G. Prete
INFN, Laboratori Nazionali di Legnaro, I-35020 Legnaro, Italy

T. Keutgen and Y. El Masri
FNRS and IPN, Université Catholique de Louvain, B-1348 Louvain-la-Neuve, Belgium

Z. Majka
Jagellonian University, M Smoluchowski Institute of Physics, PL-30059, Krakow, Poland

A. Ono
Department of Physics, Tohoku University, Sendai, Japan
(Received 28 February 2006; published 3 January 2007)

Experimental analyses of moderate-temperature nuclear gases produced in the violent collisions of 35 MeV/nucleon ^{64}Zn projectiles with ^{92}Mo and ^{197}Au target nuclei reveal a large degree of α particle clustering at low densities. For these gases, temperature- and density-dependent symmetry energy coefficients have been derived from isoscaling analyses of the yields of nuclei with $A \leqslant 4$. At densities of 0.01 to 0.05 times the ground-state density of symmetric nuclear matter, the temperature- and density-dependent symmetry energies range from 9.03 to 13.6 MeV. This is much larger than those obtained in mean-field calculations and reflects the clusterization of low-density nuclear matter. The results are in quite reasonable agreement with calculated values obtained with a recently proposed virial equation of state calculation.

I. INTRODUCTION

In a recent theoretical article, Horowitz and Schwenk reported the development of a virial equation of state (VEOS) for low-density nuclear matter [1]. This virial equation of state is a thermodynamically consistent equation of state, in which the virial coefficients for nucleon-nucleon, nucleon-α, and α-α interactions are derived directly from experimental binding energies and scattering phase shifts. It is argued that contributions from ^{3}H and ^{3}He are expected to be small and they are ignored in the calculation. In the work reported in Ref. [1] these virial coefficients were then used to make predictions for a variety of properties of nuclear matter over a range of density, temperature, and composition. The authors view this virial equation of state, derived from experimental observables, as model independent and therefore as a benchmark for all nuclear equations of state at low densities. Its importance in

both nuclear physics and in the physics of the neutrino sphere in supernovae is discussed in the VEOS article [1]. A particularly important feature of the VEOS, emphasized in Ref. [1], is the natural inclusion of clustering that leads to large symmetry energies at low baryon density.

In this article we extend our investigations of the nucleon and light cluster emission that occurs in near-Fermi energy heavy-ion collisions [2–6] to investigate the properties of the low-density participant matter produced in such collisions. The data provide experimental evidence for a large degree of α clustering in this low-density matter, in agreement with theoretical predictions [1,7–9]. Temperature- and density-dependent symmetry free energies and symmetry energies have been determined at densities of $0.05\rho_0$ or less, where ρ_0 is the ground-state density of symmetric nuclear matter, by application of an isoscaling analysis [10,11]. The symmetry energy coefficient values obtained, 9.03 to 13.6 MeV, are much larger then those derived from effective interactions in mean-field models. The values are in reasonable agreement with those calculated in the VEOS treatment of Ref. [1].

II. EXPERIMENTAL PROCEDURES

The reactions of 35A MeV ^{64}Zn projectiles with ^{92}Mo and ^{197}Au target nuclei were studied at the K-500 Super-

---
[*]Now at Institute of Physics, Silesia University, Katowice, Poland.

[†]Now at Institute of Modern Physics Chinese Academy of Science, Lanzhou 73, People's Republic of China.

[‡]Now at Shanghai Institute of Nuclear Research, Chinese Academy of Sciences, Shanghai 201800, China.

[§]Now at Institute for Nuclear Research, Russian Academy of Sciences, RU-117312 Moscow, Russia.

Conducting Cyclotron at Texas A&M University, using the 4π detector array NIMROD [3]. NIMROD consists of a 166-segment charged-particle array set inside a neutron ball. The charged-particle array is arranged in 12 concentric rings around the beam axis. In those rings, the individual segments are fronted by ionization chambers (IC) filled with 30 Torr of CF_4 gas. Front and back windows were made of 2.0-μm aluminized Mylar foil. In each of these forward rings, two of the segments have two Si detectors(150 and 500 μm thick) between the IC and CsI detectors (super telescopes) and three have one Si detector (300 μm thick). Each super telescope is further divided into two sections. The CsI detectors are 10-cm-thick Tl doped crystals read by photomultiplier tubes. For these detectors, a pulse-shape discrimination method is employed to identify light particles. In all telescopes particles are identified in atomic number. In the super telescopes, all isotopes with atomic number $Z = 10$ are clearly identified.

The energy calibration of the Si detectors was carried out using α particles from a ^{228}Th source and the observed punch through energies of identified reaction products. Because the energy losses of the lighter particles, in particular the high-energy hydrogen isotopes, are rather small in the Si detectors, evaluation of the energy deposited in the CsI crystal from the energy loss in the Si detectors requires special care for higher-energy particles. Therefore, an additional energy calibration was performed employing Si detectors of thickness 1 mm, backed by CsI detectors of three different lengths (1, 3, and 5 cm) to measure the inclusive energy spectra of light charged particles from the reaction ^{64}Zn$+^{92}$Mo at $47A$ MeV. The energy spectra were measured at all angles corresponding to those of the 12 rings of NIMROD. The combination of thicker Si E detectors and observation of high-energy punch-through points for the particles that traversed these thinner CsI detectors allowed us to determine the energy spectra with a high degree of confidence. We then used the ^{64}Zn$+^{92}$Mo at $47A$ MeV as a standard reaction to determine the CsI energy calibrations for all other runs. Neutron multiplicity was measured with the 4π neutron detector surrounding the charged-particle array. This detector, a neutron calorimeter filled with gadolinium doped pseudocumene, consists of two hemispherical end caps and a cylindrical midsection. The midsection is divided into four separate 90-degree quadrants. The hemispheres are 150 cm in diameter with beam pipe holes in the center and they are upstream and downstream of the charged-particle array. Thermalization and capture of emitted neutrons in the ball leads to scintillation, which is observed with phototubes providing event-by-event determinations of neutron multiplicity but little information on neutron energies and angular distributions. Further details on the detection system, energy calibrations, and neutron ball efficiency may be found in Ref. [3].

III. DATA ANALYSIS

An inspection of the two-dimensional arrays depicting the detected correlation between charged-particle multiplicity and neutron multiplicity in NIMROD (not shown) reveals a distinct correlation in which increasing charged-particle multiplicity is associated with increasing neutron multiplicity.

Although there are significant fluctuations reflecting both the competition between different decay modes and the neutron detection efficiencies, these correlations provide a means for selecting the higher-multiplicity, more violent collisions. For the analysis reported in this article, we have selected events corresponding to the largest observed neutron and charged-particle multiplicities. For ^{64}Zn$+^{197}$Au at $35A$ MeV this selection corresponded to 442,000 events, whereas for ^{64}Zn$+^{92}$Mo at $35A$ MeV it corresponded to 280,000 events. Many of the techniques applied in this analysis have been discussed previously in greater detail in Refs. [3–6]. The detected correlation between charged-particle multiplicity and neutron multiplicity in NIMROD provides a means for selecting the collision violence [3–6]. For the systems studied, Ref. [3] also contains an extensive comparison of earlier experimental results with predictions of antisymmetrized molecular dynamics calculations (AMD-V) [12].

For the selected events we carried out analyses using three-source fits to the observed energy and angular distributions of the light charged particles. The assumed sources are the projectile-like fragment source (PLF), the targetlike fragment source (TLF), and an intermediate velocity (IV) source [13–16]. Even though the system evolves in a continuous fashion, such source fits provide a useful schematic picture of the emission process. From the fits we obtained parameters describing the ejectile spectra and multiplicities that can be associated to the three different sources. As in the earlier works, the IV source is found to have a source velocity very close to half of that of the projectile reflecting the initial decoupling of the momentum sphere of the participant matter from that of the remaining nucleons. This important feature of the dynamically evolving system manifests itself as kinematic differences between the early emitted light ejectiles (gas) and the remaining matter (liquid). In the following we probe the properties of this early ejectile gas as the system relaxes toward equilibrium and the two momentum spheres become more and more similar.

Treatment of the early cluster emission in a coalescence framework [17,18] has proven to be a very effective tool for understanding the energy spectra of the light ejectiles [13,14]. We have previously developed extensions of these techniques to probe the early interaction zone and dynamic evolution in Fermi-energy collisions [2,6,19,20]. For the present work we have derived information on the early thermalization stage of the reaction [2,4,19,20] by focusing on the properties of early emitted midrapidity particles associated with the IV source. Such a selection minimizes contributions from the other sources. In addition, yields assigned to the TLF source are subtracted from the experimental yields. Thus, the yields of higher-energy particles are relatively uncontaminated by later emission processes. AMD-V calculations reported previously [3,4] indicate that the velocities of early emitted light particles decrease rapidly with increasing average emission time. We have examined the evolution of the system by determining various parameters characterizing the ejectile yields, i.e., temperature, α mass fraction, N/Z ratios, and isoscaling parameters, as a function of ejectile velocity. The velocity employed is the "surface velocity," V_{surf}, of the emitted particles in the IV frame, defined as the velocity of an emitted

species at the nuclear surface, prior to acceleration in the Coulomb field [13]. The energy prior to Coulomb acceleration is obtained in our analysis by subtraction of the Coulomb barrier energy derived from the source fits. In earlier studies we have employed the calculated correlation from AMD-V predictions to calibrate the timescale associated with our data [2,4,5,20].

IV. TEMPERATURE DETERMINATIONS

To characterize the temperature evolution of the system we have used the yields of ^{2}H, ^{3}H, ^{3}He, and ^{4}He clusters to determine the double isotope temperature, T_{HHe}, as a function of V_{surf} in the IV frame [21,22].

$$T_{\text{HHe}} = \frac{14.3}{\ln\left[\sqrt{(9/8)}(1.59 R_{V_{\text{surf}}})\right]}, \quad (1)$$

where $R_{V_{\text{surf}}}$, the double ratio of cluster yields, Y, for clusters with the same surface velocity, is $[Y(^2\text{H})\ Y(^4\text{He})]/[Y(^3\text{H})\ Y(^3\text{He})]$ and the constants 14.3 and 1.59 reflect binding energy, spin, masses, and mass differences of the ejectiles. Equation (1), for particles with the same V_{surf}, differs from the usual formulation by a factor of $\frac{9}{8}^{\frac{1}{2}}$ appearing in the logarithmic term in the denominator [4].

We present, in Fig. 1, results for the double isotope ratio temperatures as a function of surface velocity in the intermediate velocity frame. These temperatures have previously been reported in Ref. [4]. The temperature evolution of the IV source ejectiles is seen to be quite similar for the two different systems. For each system investigated the double isotope ratio temperature determination exhibits a high maximum temperature, near 13 MeV. In each case, after reaching a maximum the temperature then decreases monotonically as the velocity decreases. In Refs. [4,5] we discuss this evolution and present varying pieces of evidence that at velocities smaller than the peak velocity, the system attains chemical equilibrium, at least on a local basis. This appears to occur at times near 115 fm/c. Entry into the evaporation stage of the reaction occurs at V_{surf} near 3 cm/ns, corresponding to times near 160 fm/c. At that latter point, the temperatures are near 6 MeV,
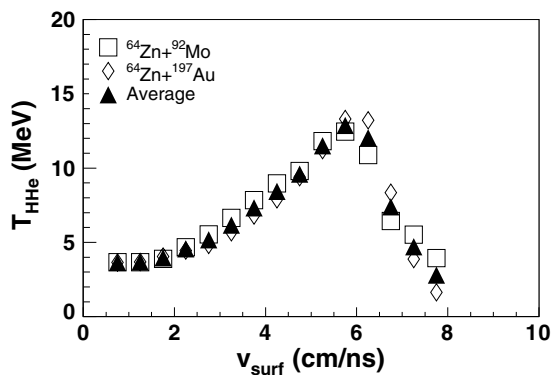
comparable to those observed in the caloric curve plateaus for these systems [23]. In the plateau region average densities (liquid plus gas) as low as $0.4\rho_0$ are indicated by a previous expanding Fermi-gas analysis [24].

V. ALPHA MASS FRACTIONS

The VEOS article [1] employs the α mass fraction, X_A, defined as the ratio of mass bound in α particles to the total mass of the matter under consideration, to characterize the degree of α clustering at different densities and temperatures. We have determined experimental values of X_A as a function of velocity. For this purpose it was assumed that the unmeasured neutron multiplicity at a given velocity was the product of the ^{3}H/^{3}He yield ratio times the proton yield for that velocity. For the IV souce particles this is implicit in coalescence assumptions [17–19] and consistent with experimental results [25,26]. In this way both the total mass yields and the mass fractions could be deduced. The sum of the mass emitted from the IV source is 31.9 ± 2.5 amu for the Mo target and 29.7 ± 2.4 amu for the Au target. As in the case of the temperature evolution, the close correspondence of ejected mass provides evidence of production of a similar zone of participant matter in the two different cases.

In Fig. 2 we present the results for α mass fractions for the IV source ejectiles of both systems. For the two systems X_A evolves in a similar fashion with surface velocity. As the surface velocity decreases X_A increases dramatically. X_A is smaller for the more neutron rich ^{64}Zn+^{197}Au entrance channel. Figures 1 and 2 clearly indicate that large alpha mass fractions are associated with the lower temperatures.

VI. ISOSCALING

Horowitz and Schwenk have pointed out that extensive α clustering in the low-density gas leads naturally to an increase in the symmetry energy for the clustering system [1]. For comparison to the symmetry energy predictions of the VEOS model we have derived symmetry energies from the ejectile yield data by employing an isoscaling analysis. Such
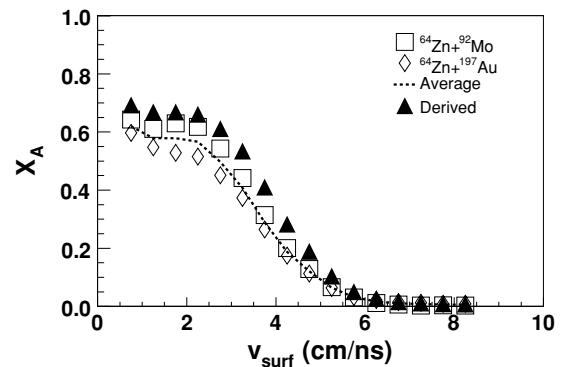

FIG. 1. Double isotope ratio temperatures, T_{HHe}, as a function of surface velocity for 35 MeV/nucleon ^{64}Zn+^{92}Mo (open squares) and ^{64}Zn+^{197}Au (open diamonds). Also shown is the average of the two (solid triangles). Uncertainties are estimated to be $\leqslant 30\%$

FIG. 2. Alpha mass fractions, X_A, as a function of surface velocity for 35 MeV/nucleon ^{64}Zn+^{92}Mo (squares) and ^{64}Zn+^{197}Au (diamonds). Also shown by the dashed line is the average of the two. Solid triangles represent derived values used for comparison to VEOS results. See text.

analyses have been reported in a number of recent articles [10,11,27–30]. In this approach the yields of a particular species $Y(N, Z)$ from two different equilibrated nuclear systems, 1 and 2, of similar temperature but different neutron to proton ratios, N/Z, are expected to be related through the isoscaling relationship

$$\frac{Y_2}{Y_1} = Ce^{\{[\mu_2(n)-\mu_1(n)]N+[\mu_2(p)-\mu_1(p)]Z\}/T} \quad (2)$$

$$= Ce^{\alpha N+\beta Z}, \quad (3)$$

where C is a constant and $\mu(n)$ and $\mu(p)$ are the neutron and proton chemical potentials.

The isoscaling parameters $\alpha = [\mu_2(n) - \mu_1(n)]/T$ and $\beta = [\mu_2(p) - \mu_1(p)]/T$, representing the difference in chemical potential between the two systems, may be extracted from suitable plots of yield ratios. Either parameter may then be related to the symmetry free energy, F_{sym}. With the usual convention that system 2 is richer in neutrons than system 1,

$$\alpha = 4F_{sym}[(Z_1/A_1)^2 - (Z_2/A_2)^2]/T \quad (4)$$

$$\beta = 4F_{sym}[(N_1/A_1)^2 - (N_2/A_2)^2]/T, \quad (5)$$

where Z is the atomic number and A is the mass number of the emitter. Thus, F_{sym} may be derived directly from determinations of system temperatures, Z/A ratios, and isoscaling parameters. We emphasize that the present analysis is carried out for light species characteristic of the nuclear gas rather than, as in most previous analyses, for the intermediate mass fragments thought to be characteristic of the nuclear liquid.

In previous works attempts were made to employ systems of similar Z and derive the α parameter, which is expected to be less sensitive to Coulomb effects. It is normally assumed that all contributions to F_{sym} other than that arising from the symmetry energy, e.g., bulk, Coulomb, and surface, may be ignored [10,11,27–30]. Most commonly, the expression,

$$\alpha = 4\gamma[(Z_1/A_1)^2 - (Z_2/A_2)^2]/T, \quad (6)$$

in which γ is the symmetry energy coefficient, has been employed with estimates of Z_1/A_1, Z_2/A_2, and T to obtain estimates of γ [10,11,27–30]. Although the approximate Eq. (6) may be reasonable for systems near normal density, it becomes increasingly less accurate at low densities where entropic effects become increasingly more important [31]. Indeed a recent article demonstrated the existence of isoscaling effects in a noninteracting system with no symmetry energy, resulting entirely from maximal entropy [31]. Further, the VEOS treatment indicates that clustering in low-density matter leads to entropic contributions to the free energy that can differ significantly in magnitude and even in sign from those obtained from mean-field calculations [1]. In this work we employ Eq. (4) with experimentally determined isoscaling parameters, temperatures, and Z/A ratios to determine the symmetry free energy, F_{sym}. We believe the present work to be the first isoscaling analysis in which all relevant parameters of Eqs. (4) and (5) have been determined experimentally. We then employ calculated entropic corrections from Ref. [1] to obtain the symmetry energy, E_{sym}.
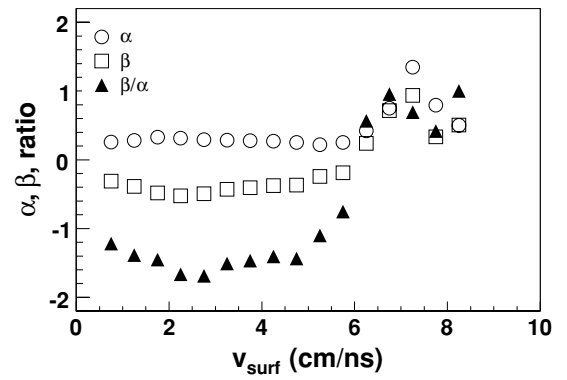

FIG. 3. Isoscaling parameters as a function of surface velocity. The values for the parameters α (open circles), β (open squares), and the parameter ratio α/β (solid triangles). Estimated errors are $\pm 5\%$

VII. ISOSCALING PARAMETERS, α AND β

The isoscaling analysis of the two systems was done in the usual way by plotting isotope or isotone yield ratios, in our case for $Z = 1$ and $Z = 2$ particles, and doing a global fit to the yield ratios to obtain α and β. In Fig. 3, the isoscaling parameters, α and β, are plotted against surface velocity.

We see that below 5.0 cm/ns the values vary slowly. Below 5 cm/ns the ratio, α/β, also varies slowly but increases dramatically at higher velocities, even changing sign. We have previously suggested that equilibration is observed for velocities below those for which the peak temperatures are seen. In our opinion the behavior of the individual parameters and of the α/β ratio provides further evidence that equilibration is achieved for surface velocities below 5 cm/ns.

VIII. Z/A RATIOS

For each emitting system, the sums of Z and A for the emitted ejectiles, taken to be characteristic of that of the sampled gas, have been derived as a function of surface velocity. From these the values of $[(Z_1/A_1)^2-(Z_2/A_2)^2]^2$ were then obtained. These values are presented in Fig. 4 as a function of surface velocity. For comparison, theoretical values obtained for the gas fraction derived from the AMD-V
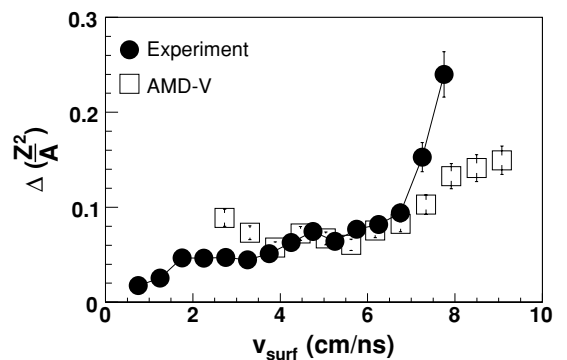

FIG. 4. The quantity $[(Z_1/A_1)^2-(Z_2/A_2)^2]^2$ as a function of surface velocity. Experimental determinations are represented by solid circles. Results of AMD-V calculations are represented by open squares.

TABLE I. Temperatures, densities and symmetry energies.

V_{surf} (cm/ns)	T (MeV)	F_{sym} (MeV)	ρ (nuc/fm^3)	E_{sym} (MeV)
0.75	3.65	5.40	0.00184	9.03
1.25	3.68	5.67	0.00147	9.66
1.75	3.97	6.69	0.00213	11.1
2.25	4.56	7.63	0.00355	11.9
2.75	5.18	8.11	0.00453	12.1
3.25	6.16	9.73	0.00488	13.6
3.75	7.33	11.3	0.00566	13.6
4.25	8.44	11.7	0.00675	13.4
4.75	9.60	12.2	0.00604	12.8

calculation are also presented. The experimental results and those for the gas in the dynamical AMD-V calculation are generally quite close in the 3- to 7-cm/ns surface velocity.

IX. SYMMETRY FREE ENERGIES AND DENSITIES

Experimentally determined values of T, Z/A, and α were used in Eq. (4) to calculate F_{sym} as a function of surface velocity. (Note that both temperature and density are varying with surface velocity.) The values of F_{sym} are presented in column 3 of Table I. Values of range from 12.2 to 5.4 MeV as the surface velocity decreases from 4.75 to 0.75 cm/ns.

Although densities are not easily accessible experimental quantities in collision studies, knowledge of the densities at which the F_{sym} determinations are being made is critical to an interpretation of the measured values.

As pointed out by Albergo *et al.* knowledge of the temperature allows the extraction of the free proton densities from the yield ratios of ejectiles that differ by one proton, e.g., the yield ratio of ^{4}He to ^{3}He. Specifically,

$$\rho_p = 0.62 \times 10^{36} T^{3/2} e^{-19.8/T} Y(^4\text{He})/Y(^3\text{H}). \quad (7)$$

Here T is the temperature in MeV, Y refers to the yield of the species under consideration, and ρ_p has units of nucleons/cm^3.

Correspondingly, the free neutron densities may be extracted from the yield ratios of ejectiles which differ by one neutron. Specifically,

$$\rho_n = 0.62 \times 10^{36} T^{3/2} e^{-20.6/T} Y(^4\text{He})/Y(^3\text{He}). \quad (8)$$

Once the free nucleon densities are known, the densities of the other particles may be calculated from the experimentally observed yields. This, again, is done as a function of surface velocity. The results, obtained by summing the densities of particles with $A = 1$ to 4, for the two reaction systems, are presented in Fig. 5. The values for the two systems show quite good agreement and indicate low densities. It is worth noting that our measurements of both the temperature and the associated α mass fraction, X_α, also provide a means of estimating the densities by comparison with the Schwenk and Horowitz [1] or Shen *et al.* [9] calculations. Like the Albergo calculation these calculations assume chemical equilibrium and lead to similar low densities.
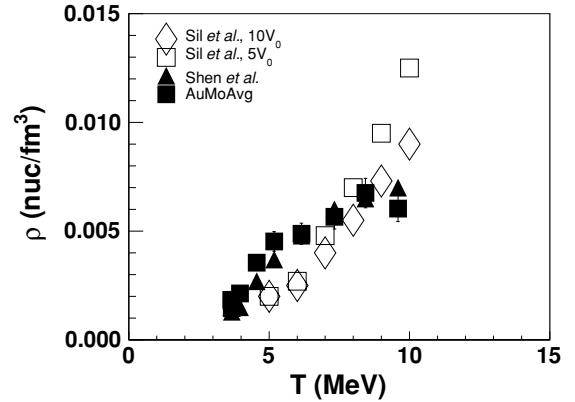

FIG. 5. Estimated nuclear densities as a function of temperature. Values derived from the experimental yield ratios using the Alberga formulas are indicated by solid squares. Theoretical results from Ref. [21] are shown by solid triangles. Values derived from the theoretical calculations of Ref. [32] are shown for confining volumes of 5 V_0 (open squares) and 10 V_0 (open diamonds).

For the higher temperatures and densities, where the Shen *et al.* calculations include competition from heavier species, the Shen *et al.* calculation indicates slightly higher densities for a given temperature and α mass fraction. In the following analysis we employ the densities from the Albergo model treatment. The resultant densities, presented in column 4 of Table I and in Fig. 5, range from 1.5 to 7.0 $\times$ 10^{-3} nucleons/fm^3. For comparison to these values we also show in Fig. 5 theoretical results reported by Sil *et al.* [32] for hot Thomas-Fermi model calculations for ^{185}Re confined in volumes of 5 or 10 times V_0, the nuclear volume at normal density. At temperatures of 5 to 10 MeV, they found average gas (or low density surface matter) densities in the range of 2 to 10×10^{-3} nucleons/fm^3. Below $T = 10$ MeV these values are in good agreement with those derived from comparison of the data to the VEOS results and provide some support for those derived from the experiment. In an earlier application of the virial equation approach to similar types of reactions, Pratt *et al.* [33] derived densities of $1-3 \times 10^{-3}$ nucleons/fm^3 and temperatures of 4.38 to 7.90 MeV. These are in the range of the present results. Additionally, it is worth noting that the derived gas densities at the temperatures in Table I are quite similar to those indicated by recent Fisher scaling model analyses of fragmentation data by Elliott *et al.* [34].

It is also possible to estimate gas densities using AMD-V model calculations once a calculational criterion capable of distinguishing gas nucleons from liquid nucleons is established. For this calculation, we first verified that the parametrization of the AMD-V model reproduced, at 300 fm/c, a total mass fraction of gas, i.e., of particles with $A \leqslant 4$, in reasonable agreement with that derived from the experiment. Although clusters are naturally produced in AMD-V calculations, early recognition of clusters relies on a physical space coalescence radius parameter. The value of 2.5 fm was used in this calculation. We then calculated, as a function of time, the average separation distance between all nucleons assigned to the gas. From the average separation distance the average density is readily derived assuming spherical

symmetry in the source frame. The AMD-V derived densities, averaged for Mo and Au targets, are in the range of 2 to 4 × 10^{-3} nucleons/fm^3. The agreement between the AMD-V results and these experimental values in Fig. 5, although not perfect, is reasonable, particularly when it is recognized that the AMD-V results demand a separation of nucleons for identification as "gas," whereas the clustering may actually occur in a slightly higher density surface region of matter identified as "liquid" by the AMD-V analysis. Thus the results depend on the early recognition coalescence parameter.

X. ENTROPIES AND SYMMETRY ENERGIES

For the densities and temperatures derived from our data, we employed the entropy equations of the VEOS calculation to determine the temperature- and density-dependent entropic contribution to F_{sym}. We have done this for the densities and temperatures of Table I.

Given that the isoscaling parameter is sensitive to both the symmetry energy and symmetry entropy contributions, derivation of the temperature- and density-dependent symmetry energy coefficient from the isoscaling parameter requires an evaluation of the symmetry entropy contribution. We based our extraction of this contribution on the entropy equations of the Schwenk and Horowitz article. In that work, the entropy density is expressed as

$$s = \frac{5P}{2T} - n_n \log z_n - n_p \log z_p - n_\alpha \log z_\alpha \quad (9)$$

$$+ \frac{2T}{\lambda^3}\left[(z_n^2 + z_p^2)b'_n + 2z_p z_n b'_{pn}\right] \quad (10)$$

$$+ \frac{T}{\lambda_\alpha^3}\left[z_\alpha^2 b'_\alpha + 2z_\alpha(z_n + z_p)b'_{\alpha n}\right], \quad (11)$$

where P is the pressure; n_n, n_p, and n_α are the n, p, and α-particle densities; z_n, z_p, and z_α are the particle fugacities; $\lambda(\lambda_\alpha)$ denotes the nucleon (α-particle) thermal wavelength; and the b_i terms denote the temperature derivatives of the second virial coefficients [1].

The entropy per nucleon is then

$$\frac{S}{A} = \frac{s}{n_b}, \quad (12)$$

where n_b is the total baryon density in the gas. Given that ^{3}H and ^{3}He are observed experimentally, we add their mixing entropy terms, contributions of the type $-n_i \ln z_i$ to the entropy density equation. At the low apparent density of the nuclear gas with which we are dealing, we assume that the particle interaction terms are very small and that differences between them for the two different systems studied may be neglected. Thus we truncate the equation by dropping the interaction terms. We then replace the fugacities in the mixing entropy terms by fractional yields and calculate the entropy per nucleon for the two systems. With some scatter they exhibit an essentially linear dependence on surface velocity. Thus, we have proceeded by making a linear fit to the entropy per nucleon as a function of surface velocity for each system. We then extract the entropy difference, ΔS, between the two systems.
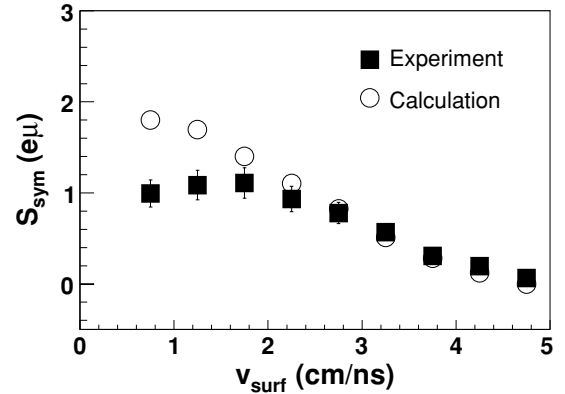

FIG. 6. S_{sym} vs v_{surf}. Experimental data are represented by closed squares and calculated values are shown by open circles.

Knowing the total neutron and proton composition for the gas in the two systems we extract the symmetry entropy coefficient, S_{sym},

$$S_{sym} = \Delta S/[(N - Z)/A]^2, \quad (13)$$

The values thus derived are presented as a function of surface velocity in Fig. 6. For comparison we also show the values calculated from the Schwenk and Horowitz VEOS for the corresponding temperatures and densities. The agreement is quite reasonable except at the very lowest density.

The symmetry energies obtained are presented in column 5 of Table I. The determination leads to values of the symmetry energy coefficients that range from 9.03 to 13.6 MeV. We estimate the overall errors of these to be ±15%. The symmetry energy coefficients are also plotted against density in Fig. 7, where they are compared to those of uniform nuclear matter that are predicted by the Gogny effective interaction [35] and to the $31.6(\rho/\rho_0)^{1.05}$ dependence suggested by a recent analysis of isospin diffusion data [36]. The derived values of E_{sym} are much higher than those predicted by mean-field calculations that ignore the cluster formation.
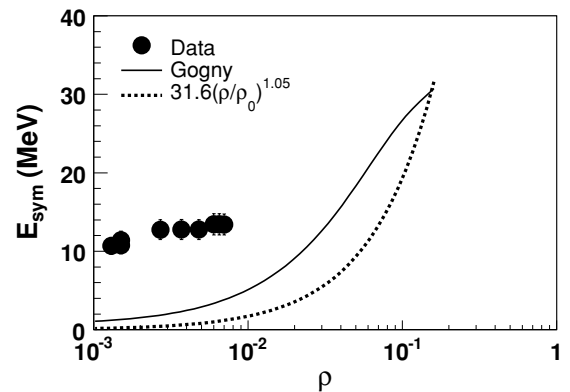

FIG. 7. Derived symmetry energy coefficients as a function of baryon density. Solid diamonds indicate results using densities of column 4 in Table I. Solid line indicates the variation predicted by the Gogny interaction. The dotted line represents the function $31.6(\rho/\rho_0)^{1.05}$ [36].

XI. CONCLUSIONS

For nuclear gases with average proton fraction, $Y_p \sim 0.44$, corresponding to the experimental average asymmetry of the Mo and Au target results and densities at and below 0.05 times normal nuclear density, experimental symmetry energy coefficients of 9.03 to 13.6 MeV, with an estimated uncertainty of 15%, have been derived from experimentally determined symmetry free energies, F_{sym}, determined using the isoscaling method. The symmetry energies are far above those obtained in common effective interaction calculations and reflect cluster formation, primarily of α particles, not included in such calculations. The entropic contributions to the symmetry free energies derived from isoscaling analyses are very important at low densities and are strongly affected by the cluster formation. The experimental values obtained agree well with the predictions of the VEOSt model proposed by Horowitz and Schwenk [1]. Inclusion of ^{3}H and ^{3}He and heavier clusters into the theoretical formalism is certainly desirable. Measurements at slightly higher densities should be more sensitive to the interaction terms in the VEOS.

[1] C. J. Horowitz and A. Schwenk, Nucl. Phys. **A776**, 55 (2006).

[2] K. Hagel *et al.*, Phys. Rev. C **62**, 034607 (2000).

[3] R. Wada *et al.*, Phys. Rev. C **69**, 044610 (2004).

[4] J. Wang *et al.*, Phys. Rev. C **72**, 024603 (2005).

[5] J. Wang *et al.*, Phys. Rev. C **71**, 054608 (2005).

[6] J. Wang *et al.*, arXiv preprint nucl-ex/0603009, Phys. Rev. C (2006), accepted in press.

[7] M. Beyer, S. A. Sofianos, C. Kuhrts, G. Roepke, and P. Schuck, Phys. Lett. **B488**, 247 (2000).

[8] M. Beyer, S. Strauss, P. Schuck, and S. A. Sofianos, Eur. Phys. J. A **22**, 261 (2004).

[9] H. Shen, H. Toki, K. Oyamatsu, and K. Sumiyoshi, Nucl. Phys. **A637**, 435 (1998); Prog. Theor. Phys. **100**, 1013 (1998).

[10] M. B. Tsang, W. A. Friedman, C. K. Gelbke, W. G. Lynch, G. Verde, and H. Xu, Phys. Rev. Lett. **86**, 5023 (2001).

[11] M. B. Tsang, W. A. Friedman, C. K. Gelbke, W. G. Lynch, G. Verde, and H. S. Xu, Phys. Rev. C **64**, 041603(R) (2001).

[12] A. Ono, Phys. Rev. C **59**, 853 (1999).

[13] T. C. Awes, G. Poggi, C. K. Gelbke, B. B. Back, B. G. Glagola, H. Breuer, and V. E. Viola Jr., Phys. Rev. C **24**, 89 (1981).

[14] T. C. Awes, G. Poggi, S. Saini, C. K. Gelbke, R. Legrain, and G. D. Westfall, Phys. Lett. **B103**, 417 (1981).

[15] D. Prindle *et al.*, Phys. Rev. C **57**, 1305 (1998).

[16] R. Wada *et al.*, Phys. Rev. C **39**, 497 (1989).

[17] L. P. Csernai and J. I. Kapusta, Phys. Rep. **131**, 223 (1986).

[18] A. Z. Mekjian, Phys. Rev. C **17**, 1051 (1978); Phys. Rev. Lett. **38**, 640 (1977); Phys. Lett. **B89**, 177 (1980).

[19] J. Cibor *et al.*, in *Isospin Physics in Heavy-Ion Collisions at Intermediate Energies*, edited by Bao-An Li and W. Udo Schroeder (NOVA Science, New York, 2001), p. 283.

[20] J. Cibor *et al.*, Phys. Lett. **B473**, 29 (2000).

[21] S. Albergo, S. Costa, E. Costanzo, and A. Rubbino, Nuovo Cimento A **89**, 1 (1985) .

[22] A. Kolomiets, V. M. Kolomietz, and S. Shlomo, Phys. Rev. C **55**, 1376 (1997).

[23] J. B. Natowitz, R. Wada, K. Hagel, T. Keutgen, M. Murray, A. Makeev, L. Qin, P. Smith, and C. Hamilton, Phys. Rev. C **65**, 034618 (2002).

[24] J. B. Natowitz, K. Hagel, Y. Ma, M. Murray, L. Qin, S. Shlomo, R. Wada, and J. Wang, Phys. Rev. C **66**, 031601(R) (2002).

[25] T. Keutgen and J. Wang (unpublished data).

[26] M. Famiano *et al.*, Phys. Rev. Lett. **97**, 052701 (2006).

[27] A. S. Botvina, O. V. Lozhkin, and W. Trautmann, Phys. Rev. C **65**, 044610 (2002).

[28] A. Ono, P. Danielewicz, W. A. Friedman, W. G. Lynch, and M. B. Tsang, Phys. Rev. C **68**, 051601(R) (2003).

[29] G. A. Souliotis, M. Veselsky, D. V. Shetty, and S. J. Yennello, Phys. Lett. **B588**, 35 (2004).

[30] A. Le Fèvre *et al.*, Phys. Rev. Lett. **94**, 162701 (2005).

[31] A. Dávila, C. Escudero, J. A. López, and C. O. Dorso, Physica A **374**, 663 (2007).

[32] T. Sil, S. K. Samaddar, J. N. De, and S. Shlomo, Phys. Rev. C **69**, 014602 (2004).

[33] S. Pratt, P. Siemens, and Q. N. Usmani, Phys. Lett. **B189**, 1 (1987).

[34] J. B. Elliott *et al.*, Phys. Rev. C **67**, 024609 (2003).

[35] J. Dechargé and D. Gogny, Phys. Rev. C **21**, 1568 (1980).

[36] L. W. Chen, C. M. Ko, and B. A. Li, Phys. Rev. Lett. **94**, 032701 (2005).